PROSTHETICS

Merging motoneuron and postural synergies in prosthetic hand design for natural bionic interfacing

Patricia Capsi-Morales[1]†, Deren Y. Barsakcioglu[2]†, Manuel G. Catalano[3], Giorgio Grioli[4], Antonio Bicchi[3,4]*‡, Dario Farina[2]*‡

Despite the advances in bionic reconstruction of missing limbs, the control of robotic limbs is still limited and, in most cases, not felt to be as natural by users. In this study, we introduce a control approach that combines robotic design based on postural synergies and neural decoding of synergistic behavior of spinal motoneurons. We developed a soft prosthetic hand with two degrees of actuation that realizes postures in a two-dimensional linear manifold generated by two postural synergies. Through a manipulation task in nine participants without physical impairment, we investigated how to map neural commands to the postural synergies. We found that neural synergies outperformed classic muscle synergies in terms of dimensionality and robustness. Leveraging these findings, we developed an online method to map the decoded neural synergies into continuous control of the two-synergy prosthetic hand, which was tested on 11 participants without physical impairment and three prosthesis users in real-time scenarios. Results demonstrated that combined neural and postural synergies allowed accurate and natural control of coordinated multidigit actions (>90% of the continuous mechanical manifold could be reached). The target hit rate for specific hand postures was higher with neural synergies compared with muscle synergies, with the difference being particularly pronounced for prosthesis users (prosthesis users, 82.5% versus 35.0%; other participants, 79.5% versus 54.5%). This demonstration of codesign of multisynergistic robotic hands and neural decoding algorithms enabled users to achieve natural modular control to span infinite postures across a two-dimensional space and to execute dexterous tasks, including in-hand manipulation, not feasible with other approaches.

INTRODUCTION

The remarkable versatility and adaptability in human motor control seem to result from using structural and computational modularity as the key organizational principle of the central nervous system (CNS) (*1*). Modularity in the generation of motor tasks is observed in the synergistic muscle control as a way of organizing the redundancy of the muscular system. Synergistic control is identified as the relatively low-dimensional space needed to explain multimuscle activations (*2*–*6*) as well as the low dimension that explains the activity of large numbers of spinal motoneurons (MNs) (*7*). The neural and muscular synergistic organization is reflected in the observed preferential combined use of body kinematics postures (*8*). It has been proposed that the design of artificial limbs should partly reproduce natural postural synergies in their mechanical structure so as to reduce the number of actuation units and simplify control.

Compared with natural/biological counterparts, state-of-the-art commercial robotic hands still show limited and poorly flexible motor skills. Conversely, postural or kinematic synergies can simplify the design of robotic hands while allowing a high level of dexterity in the coordination of multiple joints. Different from the traditional designs, multisynergistic soft robotic hands would permit the continuous mapping of different grasp patterns and their transitions. The adaptive implementation of kinematic templates in the interaction with objects, through the softness property (*9*), is key to providing versatile grasping patterns. Moreover, they can yield in-hand manipulation of objects with continuous proportional control strategies substantially simpler than those needed for fully actuated systems. For natural control of these prostheses, however, the modular organization of neural variables should be matched with the postural synergistic structure of the robotic limb.

The modular organization of descending neural inputs into neuromuscular control underlies primary functional muscle coordination patterns, whose combination generates a large number of movements [for review, see (*1*, *10*)]. Nonetheless, current understanding of the computational aspect of synergistic control is limited to the analysis of muscle activities. The number of spinal MNs is orders of magnitude greater than the number of muscles involved in a motor task. Tanzarella *et al.* (*7*) identified the synergistic grouping of MNs innervating extrinsic hand muscles. This work and other recent studies (*11*) provide a new perspective within the long-established theory of muscle synergies by changing the motor control perspective. Although in the classic muscle synergies theory the muscle is the anatomical and functional unit in the generation of movements, in this new perspective, modules of MNs are the functional units.

Here, we evolved the prototype multisynergistic hand previously used in (*12*) into a prosthetic hand with two inputs capable of continuously combining and dynamically changing two kinematic modes/synergies. Their combinations span a similar linear space of postures as those generated by the two first postural synergies observed in human hands. This design allows for the grasp and in-hand manipulation of objects of different shapes with almost full hand mobility [15 degrees of freedom (DoF)] with only two degrees of actuation (DoA) (i.e., requiring two bidirectional control signals). Grasping actions can be described by two or three postural synergies (*13*),

[1]Department of Computer Engineering, Technical University of Munich (TUM), Munich, Germany. [2]Department of Bioengineering, Imperial College of London, London, UK. [3]SoftRobotics Lab for Human Cooperation and Rehabilitation, Istituto Italiano di Tecnologia, Genoa, Italy. [4]Research Center E.Piaggio, University of Pisa, Pisa, Italy.
*Corresponding author. Email: antonio.bicchi@unipi.it (A.B.); d.farina@imperial.ac.uk (D.F.)
†These authors contributed equally to this work.
‡These authors contributed equally to this work.

which justifies the implementation of only two independent actuation signals. Further, we identified MN synergies in several hand-grasping activities, and we aligned the dimensionality of the neural and mechanical manifolds to achieve control of the robotic hand (Fig. 1).

The proposed solution was tested online with participants without physical impairment and prosthesis users (PUs). Furthermore, we integrated the prosthetic hand, real-time decoding of MN activities, and a control algorithm together with a soft socket for a proof-of-concept demonstration in three PUs. The results provide a foundation for merging neuroscientific and robotic principles, which is necessary for fully realizing synergy-driven manipulation in prosthetic hands (*14*). The integration of postural and neural synergies contributes to the creation of a framework to further investigate the modular organization of upper-limb motion control, with potential applications in assistive and rehabilitative robotics.

This work introduces scientific and technical advances in bionics (Movie 1). It shows real-time electromyography (EMG) decomposition and online identification of MN synergies, integrated into a full bionic hand. From the mechatronic design view, although synergy-based prosthetic hand designs date back 10 to 15 years (*9*), they have always used only one postural synergy. Our prosthetic hand, however, features two synergistic behaviors. This innovation enables a range of different multidigit coordinations and even in-hand manipulation, a previously unattainable goal. Last, this work validates that MN synergies and muscle synergies occupy different neural manifolds, demonstrating that MN synergies offer a more accurate description of motor action flexibility. This result provides new physiological insights and highlights the importance of analyzing neural synergy substrates with the participant in the loop.

RESULTS

Development of a multisynergistic hand

We developed the SoftHand Pro-2 as an underactuated soft prosthetic hand with two synergistic behaviors. The combination of multiple soft kinematic synergies provides a continuous workspace that can reproduce several hand postures and in-hand manipulation.

Mechanical design

The SoftHand Pro-2 exhibits a total of 15 joints mostly embedding the flexion/extension of its fingers (Fig. 2). One revolute joint is present at the thumb, accounting for its abduction. The remaining 14 joints embedded in the fingers are compliant rolling-contact element joints. Elasticity is introduced by ligaments in each joint. A single tendon moves from the palm base, connecting all the finger components, and two motors actuate the tendon, each pulling it from its two sides (see Fig. 2B). If the motors move in the opposite direction, the tendon length is shortened, and the SoftHand Pro-2 closes, exhibiting a power grasp referred to as the first synergy (Fig. 2C). If instead only one motor moves, the tendon pulls from the corresponding side, partly closing the hand and generating a rotation of the fingers from side to side, which can generate pinch to index point postures. The latter movement refers to the additional synergistic behavior explored in this design, also named the second synergy, or rotation in Fig. 2C, which corresponds to the decoupling of the first synergy. By using a single actuation tendon traversing from the base of the palm through all the finger components and exploiting the friction within the device's transmission, the SoftHand Pro-2 achieves a seamless augmentation of its movements across the synergy space. This enables the device to reach distinct points within this two-dimensional (2D) space of postures, corresponding to

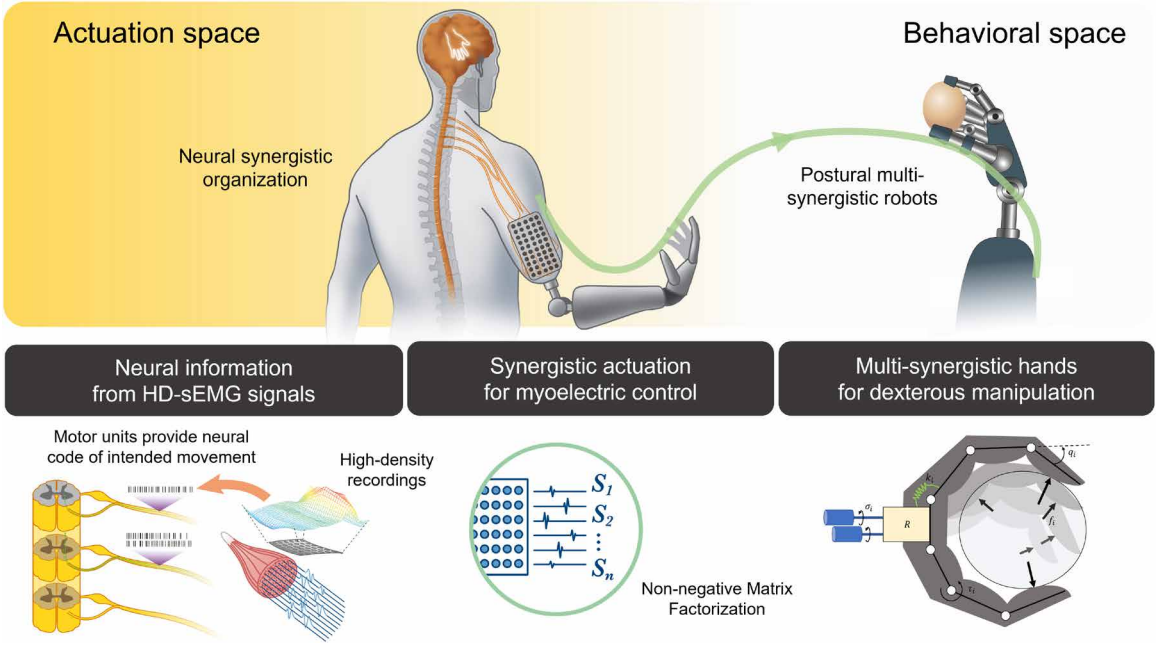

Fig. 1. Combination of postural and neural synergies for dexterous prosthetic hand control. This work explored synergies in both the behavioral and the actuation space. For natural bionic control of multisynergistic prosthetic hands, including dexterous manipulation tasks, we proposed a synergistic control approach that combines postural synergies of the prosthetic hand design with the decoded activity of spinal MNs underlying the intended movements of the fingers. The arrows in the "Multisynergistic hands for dexterous manipulation" section represent the contact forces of the object with the fingertips of the robotic hand. The angle notation q_i pertains to the kinematics of the robotic hand and defines the final geometry of the system during grasping actions.

Movie 1. Overview of the study, hand capabilities, neural decoding, and experiments with participants without physical impairment and PUs in real-time scenarios.

identifiable prehensile and non-prehensile postures. Furthermore, the soft, adaptive mechanism of the hand is such that forces are evenly distributed at contacts with objects, and the resulting shape of the hand conforms to them. The former corresponds to the notion recognized as the soft synergy model, wherein pregrasping robotic prescriptive synergies manifest in a potentially limitless array of configurations after interacting with the environment (*15*).

This prosthetic hand design, characterized by reduced dimensions and weight in comparison with earlier prototypes, is self-contained, integrating the actuation system, sensors, and a custom electronic board within the palm structure. The robotic hand includes two MAXON DC-X 16 s 12-V motors with 83:1 gearboxes mounted on the palmar area. Note that for heavy objects, power grasp is the preferred action, which is executed by the activation of both motors, so the nominal values of these motors were considered sufficient for most daily activities.

Hand capabilities

The designed prosthetic hand can perform power grasp and precision grasps such as pinch or tripod. It can also manipulate objects while maintaining a stable grasp through autonomous adaptation to the object shape (*9*). Embodied intelligence, through the designed morphology of the prosthetic hand and materials used, removes the sole reliance on control architecture (*16*). The designed prosthetic hand can perform a larger variety of grasping and manipulation tasks by combining only two DoAs with softness and synergistic behaviors (Fig. 2C). For instance, the capability of in-hand manipulation, such as for the pouring of a liquid, may be executed by exploring the two synergies at different intensity levels without any compensation at the wrist. Even though the problem of in-hand manipulation control is solved for fully actuated robotic hands (i.e., when the hand kinematics are injective), this problem is more challenging for prosthetic robotic hands (*15*). Contrary to the autonomous robotic field, however, PUs have visual feedback of the manipulated object and are in control of the positioning of the object for volitional manipulation and to correct external uncertainties. Therefore, with a natural control of the postural synergies embedded in

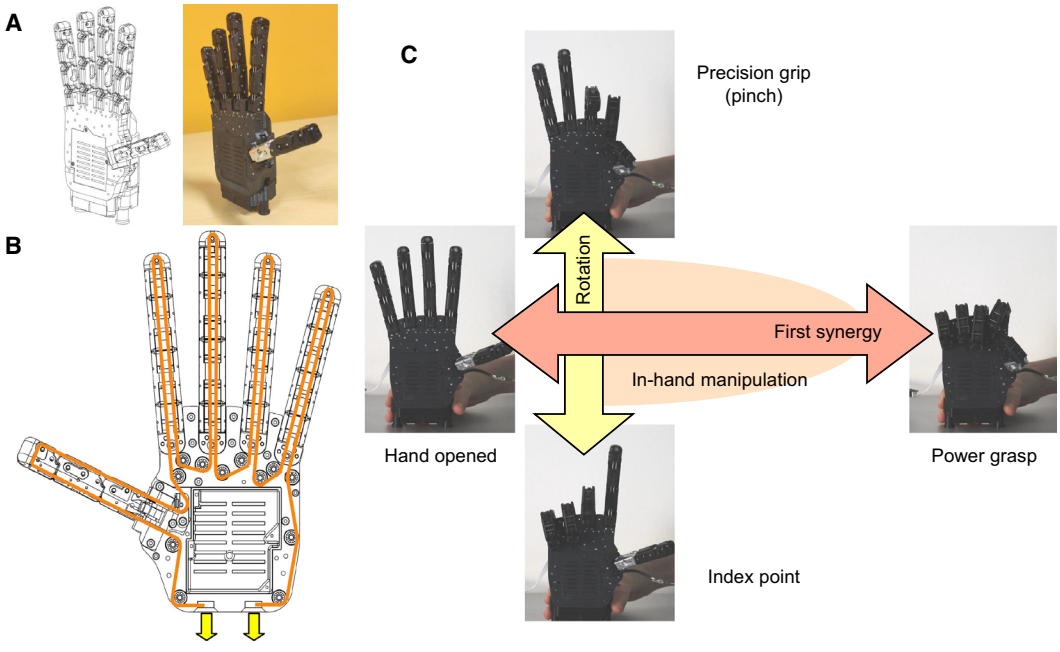

Fig. 2. Mechanical system and hardware description of the SoftHand Pro-2. (**A**) The CAD design and realization of the hand. (**B**) The routing of the system. Each side of the tendon is pulled by a DoA (represented with a yellow arrow). In this manner, all joints of the hand are actively controlled by the coordinated motion of both motors to exhibit different hand behaviors. (**C**) Theoretical workspace of the proposed framework. The vertical arrow expands the first synergy embedded in this hand processor to permit the rotation of the fingers to include additional grasping patterns and in-hand manipulation. In-hand manipulation is achieved through the counterclockwise and clockwise rotation of the fingers that results in different contact forces applied to the grasped object.

the artificial hand, the additional feature of in-hand manipulation may become a feasible capability.

Neural synergies

Each spinal MN receives inputs from corticospinal, other supraspinal, and afferent pathways, in most cases mediated by premotor interneurons. The output of populations of MNs is the result of the net excitatory input they receive, which is often correlated among motor neurons to form modules or synergies of MN activity (*7*). An MN synergy corresponds to a set of weights to multiple MNs that reduce the dimensionality of control by the CNS. Each synergy is controlled by an activation primitive, which is the net excitatory common input to the MN cluster and activates the cluster through the synergy weights. The synergistic organization of MN activation can be identified by factorization algorithms applied to the output spike trains of experimentally identified MN activities. Figure 3 shows a representative example of the computation pipeline for identifying MN synergies (Fig. 3, A to D) and muscle synergies (Fig. 3, A, E, and F) For MN synergies (Fig. 3D), the matrix **W** comprises the time-invariant weights of the synergies observed in 63 motor units (MUs). The matrix **H** represents the activation signals. This example illustrates that certain MUs could be recruited across various hand postures, whereas distinct groups of MUs are specific to individual tasks and are activated solely during the execution of those tasks.

Participants without physical impairment

Offline analysis

We decoded the activity of MNs innervating the hand while nine participants (28.4 ± 3.3 years old, six males and three females) exerted isometric forces during different hand movements related to the corresponding kinematics of the prosthetic hand. We analyzed

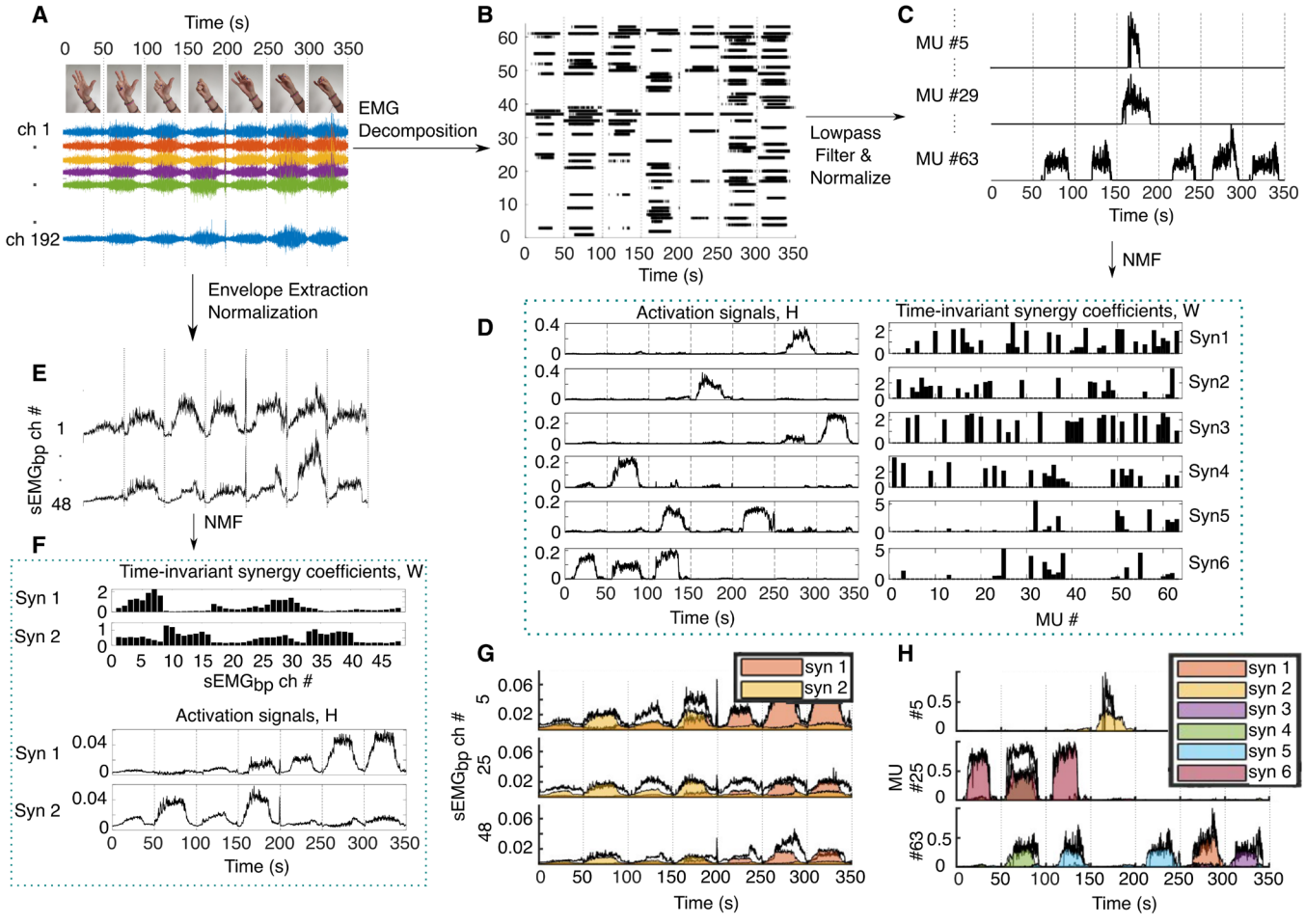

Fig. 3. MN and muscle synergy computation pipeline. (A to D) Computation of MN synergies (termed MNS in the plots). (A, E, and F) Computation of muscle synergies (termed MS in the plots). (**A**) An example of concatenated 192-channel HD-sEMG signals acquired for each hand posture. (**B**) Raster plots of the activity of the MUs decoded from the HD-sEMG signals. (**C**) Lowpass-filtered and normalized individual MU spike trains. (**D**) The plots of the activation signals (left) and time-invariant MN synergy coefficients (right) computed by the NMF algorithm. (**E**) The rectified and lowpass-filtered EMG signals. Note that in this example, the NMF was applied to 48 bipolar EMG envelopes derived from the recorded 192-channel monopolar EMG signals. (**F**) The time-invariant muscle synergy coefficients (top) and the activation signals (bottom). (**G**) An example of the reconstructed muscle activations resulting from each muscle synergy on three EMG channels (colored) and original rectified EMG signals (solid black lines) and (**H**) an example of the reconstructed MU activation patterns resulting from MN synergies on three MUs and the original SDRs (solid black lines). For (A), (C), (E), (G), and (H), only a selected subset of signals is reported for illustration purposes.

the synergies at the MU ($n = 54.11 \pm 12.05$ per participant) and muscle level by comparing dimensionality and the degree of correlation among synergies.

Dimensionality

Figure 4A shows two common methods to select the number of synergies (dimensionality) in a dataset and the fit of the factorization

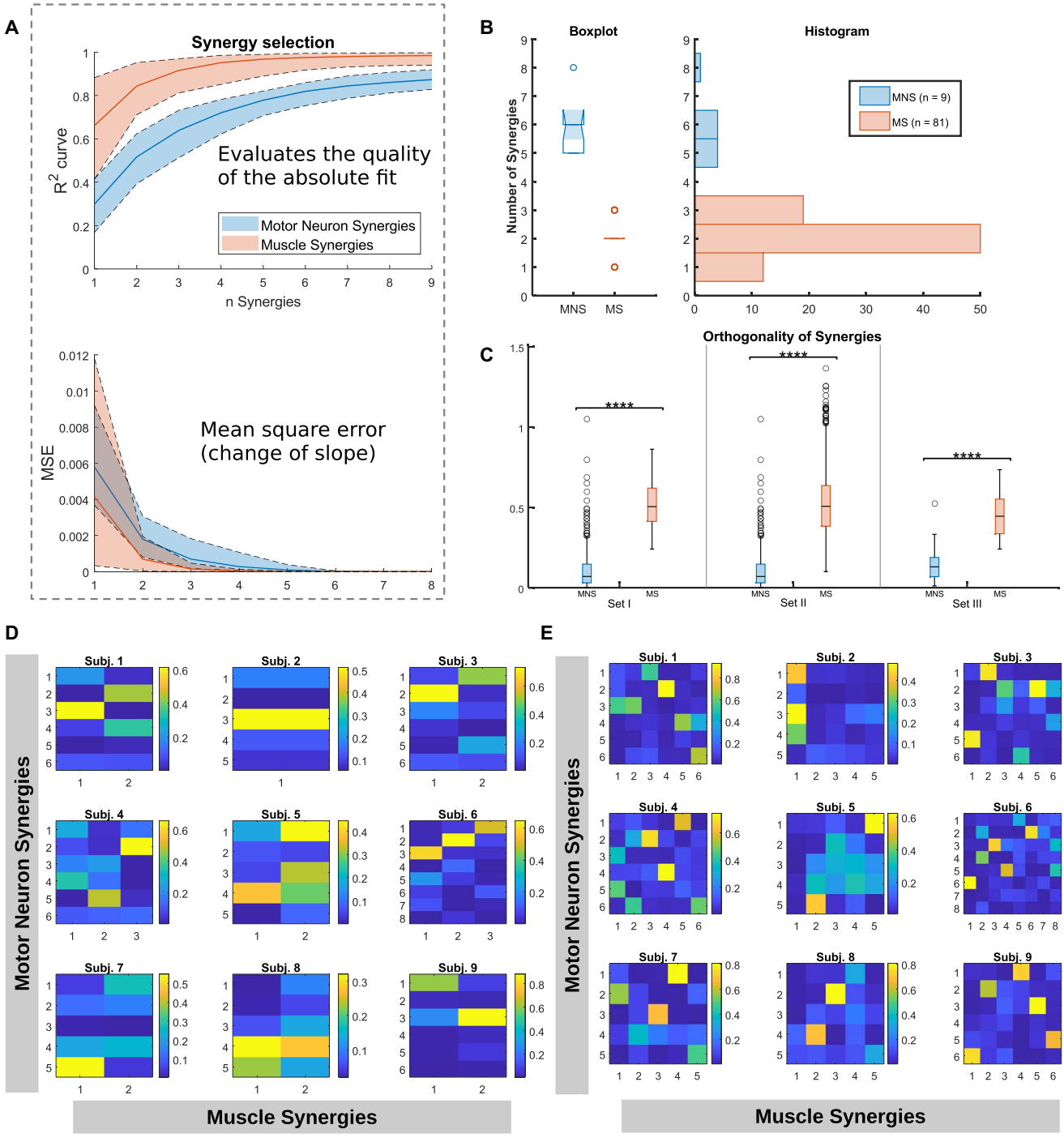

Fig. 4. Offline analysis. (**A**) Computation of synergies and the variability accounted for number of synergies according to the R^2 curve and MSE. (**B**) Dimensionality comparison between MN synergies (termed MNS in the figure) and muscle synergies (termed MS in the figure), both extracted with NMF. Note that the number of samples for muscle synergies is substantially higher. For each participant, we tried nine different sensor configurations (minimum of 12 bipolar to 192 monopolar) to determine the ideal configuration for the extraction of muscle synergies during the online experiments. (**C**) Specificity analysis between MN and muscle synergies. From left to right: set I, set II, and set III. Asterisks indicate the significance between MNS and MS groups after a two-sample *t* test, with **** referring to the statistically significant difference with $P \leq 0.0001$. (**D**) Degree of similarity between MN and muscle synergies in set I, for each participant, which indicated shared and missing information. (**E**) Degree of similarity between MN and muscle synergies in set II, to observe the common information when the dimensionality of synergies is matched in number.

output with the original data. The two methods are based on the R^2 curve and the mean square error (MSE) and were both used for the subsequent analyses. The number of synergies was estimated from the R^2 curve with a cutoff threshold of 0.8 and from the MSE with a threshold of 5×10^{-4}. For both methods, neural synergies resulted in greater dimension than muscle synergies (Fig. 4A). Figure 4B shows the distribution of the number of synergies identified with the R^2 curve for all participants and trials (5.78 ± 0.97 MN synergies versus 2.09 ± 0.62 muscle synergies).

Specificity analysis among synergies

We calculated the degree of orthogonality among pairs of synergies in an intraparticipant study to evaluate their correlation and the specificity of the information provided by each synergy. Details of this analysis can be found in Materials and Methods. A high degree of orthogonality implies that synergies are specific, with low redundancy in the synergy representation. The set of synergies obtained with the R^2 curve resulted in the largest pairwise orthogonality. Moreover, when matched in number, the MN synergies showed a higher degree of orthogonality than muscle synergies (two-sample t test, $P \leq 0.0001$). The average scalar product for intraparticipant MN synergies was 0.090 ± 0.035.

Information content of muscle and neural synergies

We analyzed the information content of MN and muscle synergies (*17*). We hypothesized that part of the information content of MN synergies was represented in muscle synergies. Cheung *et al.* (*18*) proposed a method for assessing the degree of similarity between sets of synergies using the scalar product of pairs. Here, we used a similar method to compare MN and muscle synergies. We computed the correlation of pairs of MN and muscle time-variant activation synergies (set I, see Materials and Methods) for each participant. Figure 4D shows the degree of similarity for the best-matching MN and muscle synergy pairs with a threshold of 0.9 on scalar product (*18*). Figure 4D shows that not all MN synergies could be matched with corresponding muscle synergies. Similar results were observed for the data in set II (Fig. 4E) and highlighted differences between the type and quantity of information provided by the two synergy sets.

Control of postural synergies by neural synergies

The MN synergies, derived from a limited set of hand grips, were used to develop a control framework for the SoftHand Pro-2. This framework established a continuous mapping between neural synergies and the hand postural synergies, enabling intuitive coordination of complex hand movements. Figure 5 shows the proposed method to map the synergistic activation, **H**, to the control commands of the hand, **X**. First, we examined and quantified the extent to which each MN synergy contributed to each hand task, p_i, to define the matrix $\mathbf{K} \in \mathbb{R}^{T \times S}$, where T is the number of hand patterns and S is the number of synergies. For this purpose, we considered an MN synergy active during a task if its activation signal exceeded a threshold of 10% of the maximum activity for more than 40% of the task duration. The weights, k_s, of **K,** were initialized with the average activation of each corresponding active synergy per task. Then, these were normalized per p_i by setting the sum of weights equal to 1. The trained hand postures were defined as $\mathbf{P} = \mathbf{KH}$, with dimension $T \times L$, where L is the total length of the original dataset (green area in Fig. 5), to a linear combination of **P**. Once a relation $r_{A,T}$ among p_i and the mechanics of the hand was defined (orange area in Fig. 5), $\mathbf{X} = \mathbf{RP}$ computed the final outputs **X**, with dimension $A \times L$, where A is the number of controllable DoAs, to command the prosthesis. In this work, and for the SoftHand Pro-2, **R** was defined with entries $r_{1,1} = r_{2,5} = 0.6$, $r_{1,2} = r_{2,6} = 0.7$, $r_{1,3} = r_{2,7} = 0.8$, and $r_{1,4} = r_{2,4} = 0.9$. The selection of these values corresponded to the motor command necessary to reproduce a geometry consistent with the p_i. The same procedure as described above was used to control the postural synergies with muscle synergies.

Online control

The high-density surface EMG (HD-sEMG) was decomposed in real time with a short phase of training (*19, 20*). Then, an online training version of the nonnegative matrix factorization (NMF) algorithm was applied (see Materials and Methods) to identify the synergies. The postural and neural synergies were then mapped together, as described above. During a target reaching task, 11 participants controlled a cursor within a 2D virtual space that was further mapped into the prosthesis DoA.

Figure 6A shows the comparison of the controllable workspace with MN and muscle synergies during the task of reaching 20 targets, randomly distributed in the first quadrant of the 2D virtual environment. We computed the area that covered the space that more than 50% of the participants could reach. Participants were able to control the cursor for most of the first quadrant (polygon in blue, 91.8%) matching the theoretical workspace hypothesized for MN synergies.

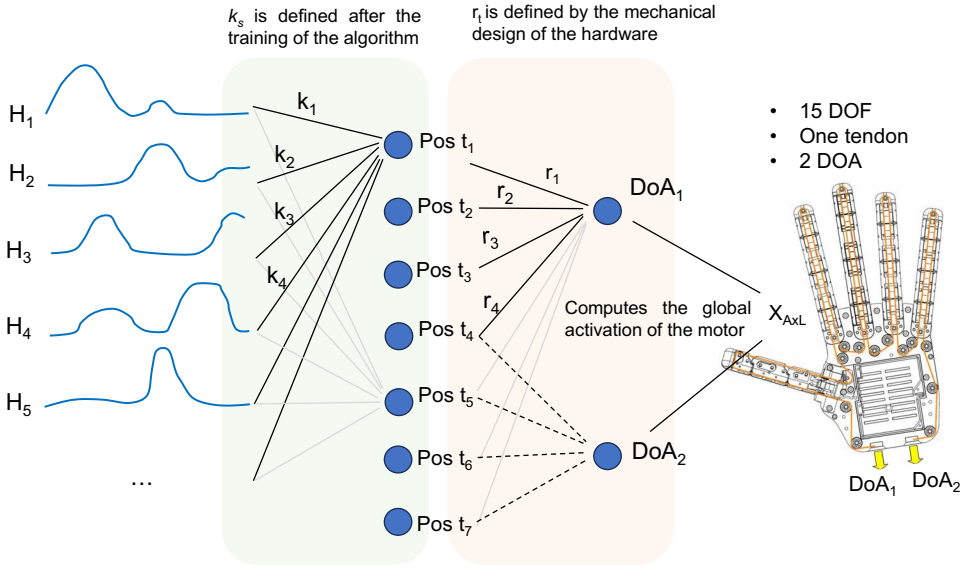

Fig. 5. The map of activation signals of the MN or muscle synergies to control inputs of the postural synergistic prosthetic hand. The synergistic activation matrix $\mathbf{H}_{S \times L}$ is related to the trained postures (matrix $\mathbf{P}_{T \times L}$, with each row named *Pos* t_i in this visualization) through the matrix $\mathbf{K}_{T \times S}$. These are then converted into the two DoAs available in the multisynergistic prosthetic hand used, termed $\mathbf{X}_{A \times L}$, for the execution hand movements. S is the number of extracted synergies, T is the number of tasks or hand postures for which the algorithm is trained, A is the number of DoAs of the robot, and L is the total length of the original dataset collected.

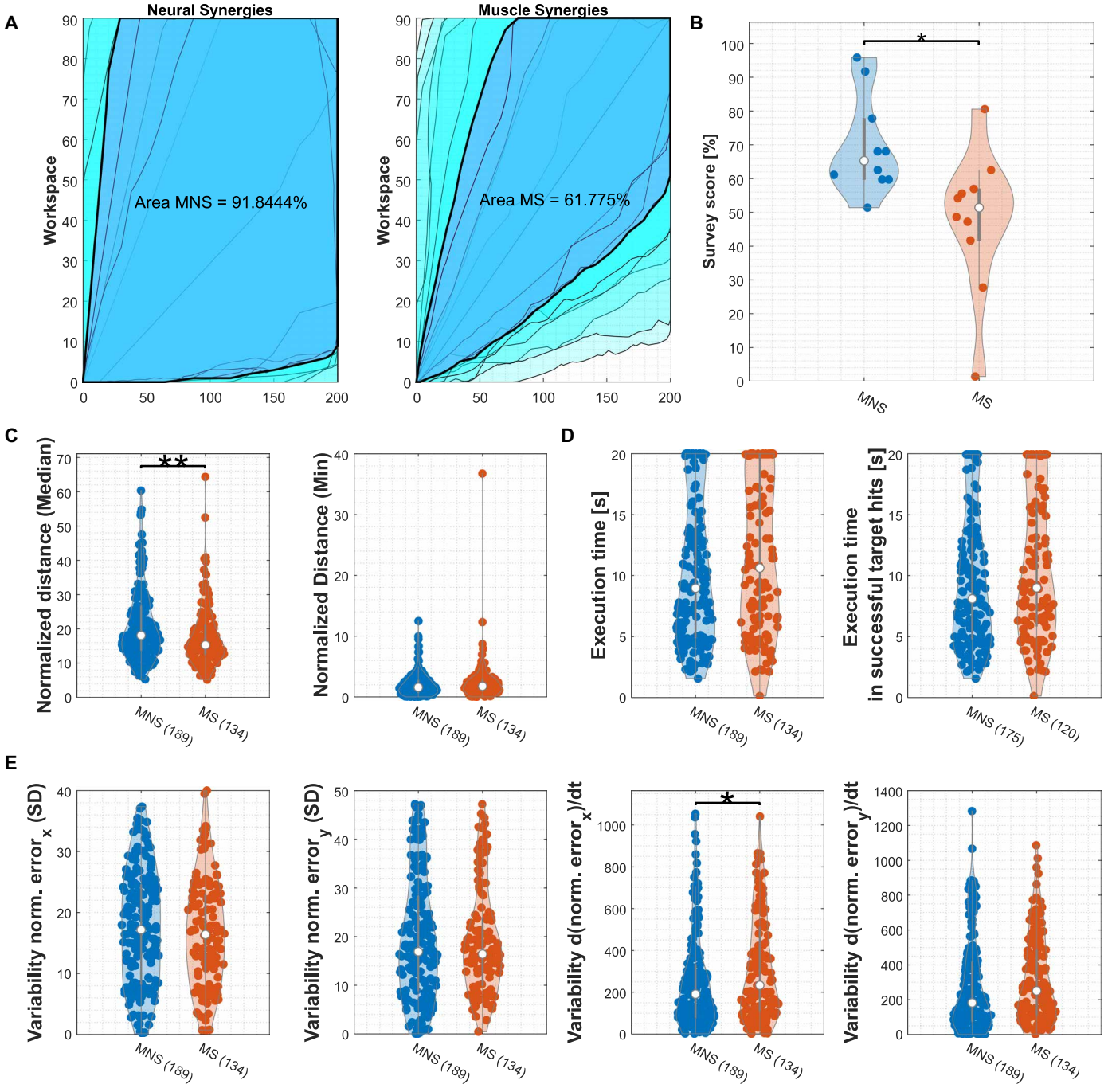

Fig. 6. Online results for controlling two synergistic DoFs with isometric muscle activations. MS refers to results for muscle synergies, and MNS corresponds to MN synergies. (**A**) The available workspace for both control conditions and each participant. A representative controllable space was computed (the dark blue area in the plot) with a set of points that were reachable in more than 6 of 11 participants. (**B**) The score (in percentage) of the self-rating survey for each control method. (**C**) Performance metrics related to the normalized distance between the commanded cursor and target to reach. This is measured in device-independent pixels. (**D**) Performance metrics related to the execution time of each target across all participants. (**E**) The variability of the cursor trajectory for each DoF is represented by the SD of the normalized error in both axes. The smoothness of the cursor trajectory in both axes is represented by the rate of change of normalized error with respect to time. All graphs report the dispersion of the data with a violin plot, with the median of each condition marked in white. A two-sample *t* test was used to compare the performance metrics between MNS and MS control conditions. Note that * refers to the statistically significant difference with $P \leq 0.05$ and ** refers to the statistically significant difference with $P \leq 0.01$. The numbers in parentheses on the *x* axis report the number of samples used for each performance metric.

Participants could reach 85.9% of the targets, including those close to the axes, that corresponded to the most distinct patterns of the hand such as pinch and index point. They were able to navigate in the space between power grasp and these distinct patterns, effectively performing in-hand manipulation. On the contrary, muscle synergies showed a more restricted workspace, covering only 61.8% of the first quadrant. As a result, participants were able to reach only 60.9% of the targets, limiting their ability to perform well-differentiated grasp patterns.

We also quantified the control performance by computing the normalized distance between the controlled cursor and the target positions (Eq. 2 in Materials and Methods). Figure 6C shows the distance results for targets that were within the reachable workspace. Although the normalized minimum distances were similar for both controllers, we observed the shortest median distance for the muscle synergies. The completion times of successful target hits, as shown in Fig. 6D, were similar for MN synergies (7.0 s) and muscle synergies (7.6 s). These results suggest similar performances of the two controllers. A slightly greater difference (0.91 s) in performance was observed when all reachable targets were considered. When only the targets reachable within the workspace were considered, MN synergies achieved a successful target hit rate of 92.6%, whereas for muscle synergies this was 89.5%. However, the reachable workspace was substantially smaller for muscle than MN synergies.

These performance metrics are comparable to results reported in the literature on more conventional control systems for prostheses (*21, 22*). However, here, the cursor movements were associated with the ability of participants to individually control finger movements proportionally and simultaneously. This is considerably more complex than standard 2D myocontrol approaches. When the analysis was not limited to the specific workspace of each control method and all targets were included, the successful target hit rate for muscle synergies was substantially lower (54.5%) than for MN synergies (79.6%). The cursor trajectory variabilities were similar for both controllers in both axes (Fig. 6E). However, MN synergy control exhibited a lower variability in the cursor error rate of change (15.7% lower for x axis and 20.7% lower for y axis) that indicated a smoother trajectory.

Participants answered a survey with multiple questions for each control method. A larger score in the survey indicated the preference of one controller over the other. The results (Fig. 6B) revealed that participants preferred MN synergies (65.3%) over muscle synergies (51.4%) for the control. Table S1 shows the survey questions and the average scores. A difference of more than one point in a five-point Likert-scale occurred in 44.4% of the questions. In all of them, participants preferred MN synergies.

Prosthesis users

Three transradial PUs participated in the study (37.3 ± 3.5 years old, three females). PU1 and PU3 were familiar with direct myoelectric control but currently wear cosmetic prostheses. PU2 was an individual with transradial amputation who underwent targeted muscle reinnervation to reduce phantom pain. At the time of the study, PU2 had been a daily user of a commercial myoelectric bionic hand for the previous 7 months.

First, we validated the proposed concept with PU1. We analyzed the number of MN synergies and compared it with the number of muscle synergies observed from 48 bipolar EMG sensors. The same electrode configuration, as in the offline conditions, was used during the online experiments. These recordings were performed under three conditions. For the first condition, the EMG signals were recorded from the intact arm while executing seven grasping actions. For the second condition, the EMG signals were recorded from the intact arm while holding a custom-designed handle to enforce isometric contractions during all tasks. For the third condition, the EMG signals were recorded from the residual limb while the intact arm mirrored the intended grasp patterns. We found five or six MN synergies in all recording conditions, proving the existence of a dimensionality of neural control similar to that in participants without physical impairment. On the contrary, only one or two muscle synergies were identified, similar to previous observations for the participants without physical impairment.

We then executed the online virtual control experiments with PU1 and PU2. The prosthesis was placed in front of PU1, and the integrated prosthetic system was worn by PU2 to relate the cursor movements with the synergistic behavior of the prosthesis. PU3 only participated in the experimental tests with the fully integrated system. Fig. 7A shows the workspace computed from the cursor movements with MN and muscle synergies for PU1 and PU2. Both PUs could explore a larger workspace with MN than muscle synergies. The results revealed that 36 of 40 targets were reachable when using the MN synergies and that 33 of 40 targets were successfully hit (Fig. 7, B to D). In comparison, when using muscle synergies, participants could reach only 16 out of the 40 targets, with 14 successful target hits. Figure 7B shows that although muscle synergies determined a lower median distance from the cursor movement to the target position, MN synergies generally required shorter times to reach the target (Fig. 7C). Moreover, Fig. 7D shows similar results on the variability of the trajectories for both control methods. Figure S1 shows results for these metrics for each individual.

Self-rating surveys were conducted to evaluate the perception of the two control methods. Figure 7E presents the survey scores for PU1 and PU2. The higher the survey score, the better the perception of the user toward the synergistic control method. Accordingly, MN synergies (with 66.7 and 80.6%) showed potential as an alternative bionic interfacing method to control multisynergistic prosthetic hands. Muscle synergies only achieved 16.7 and 27.8% for the survey scores. The survey results indicated a notable preference for MN synergies. For the questions with answers that differed by three points in a five-point Likert-scale (marked in green in table S1), we observed the following statement for muscle synergies: "(Q10) This control method is complex to use." On the contrary, for MN synergies, the participants reported the following: "(Q4) I believe this control method is easy," "(Q12) I feel confident while controlling the system," and "(Q18) I think that I would like to use this control method frequently." These answers correspond to the preferences of the participants without physical impairment.

Last, we also completed and proved the full integration of this platform by embedding HD-sEMG sensors in a soft socket (see Fig. 8, D and E), the soft multisynergistic hand and the real-time neural synergistic control for the three PUs. The prosthetic hand was equipped with an Ottobock quick disconnect prosthetic wrist for passive pronation-supination and easy integration with conventional socket interfaces. Movie S1 shows a demonstration of online control for one participant without physical limitation during grasping and in-hand manipulation of objects. Movie S2 reports the full

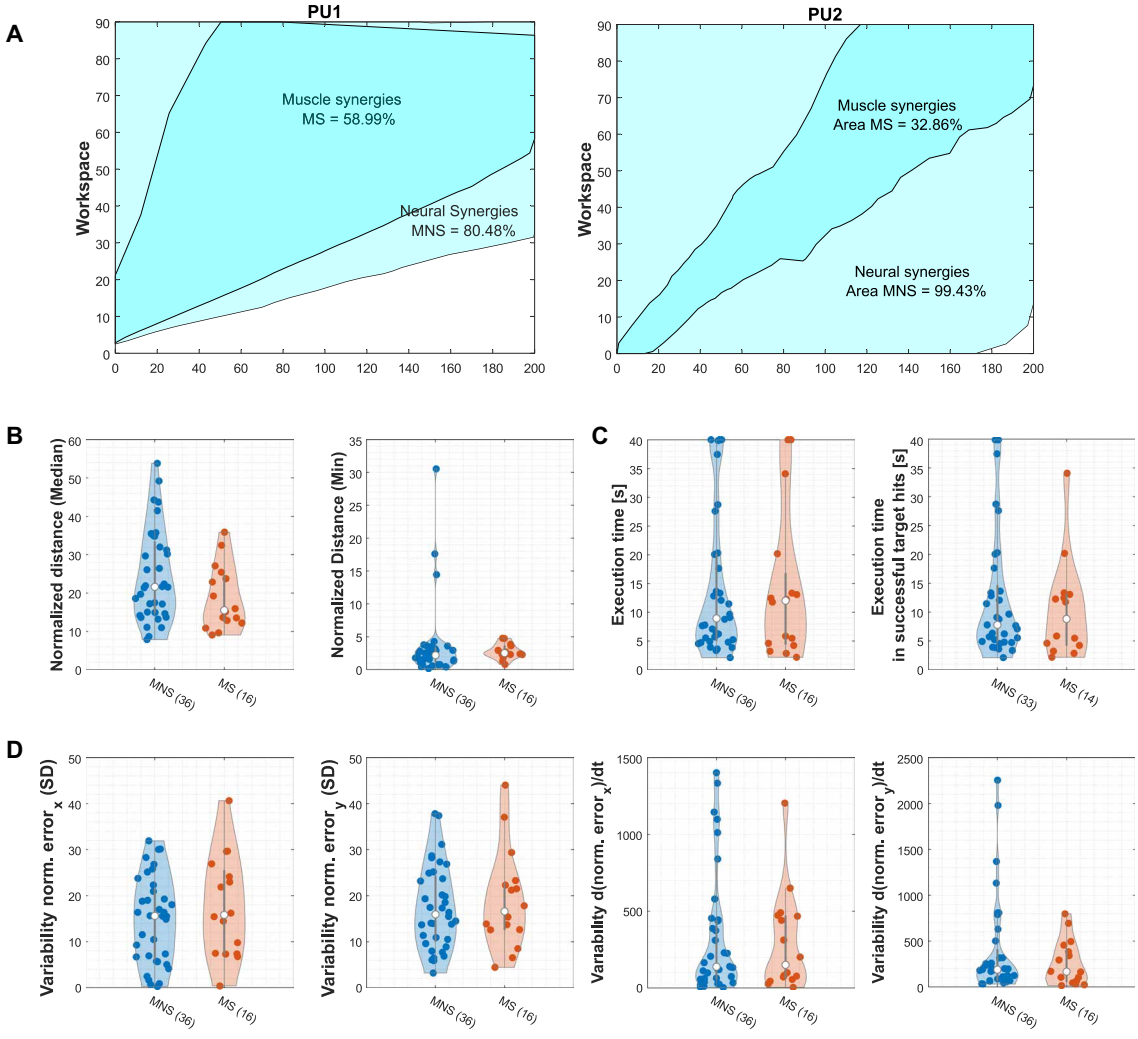

E

	PU1		PU2	
Prosthesis user	**MNS**	**MS**	**MNS**	**MS**
N inputs	16	48	30	48
Num. synergies	3	2	8	6
Workspace [%]	80.5	59.0	99.43	32.86
Reachable targets [%]	80.0	55.0	100.0	25.0
Succ. Target hits [%]	80.0	50.0	85.0	20.0
Survey [%]	66.7	16.7	80.56	27.78
Survey (questions preference [%])	88.9	5.6	77.78	5.6

Fig. 7. The results for PUs in offline and online experiments. (**A**) The reachable workspace for each control condition and its area in percentage for both participants. MS refers to the results for muscle synergies, whereas MNS corresponds to the MN synergies. (**B**) Performance metrics related to the distance between the commanded cursor and target to reach. (**C**) Performance metrics related to the execution time. (**D**) Performance metrics about the variability of the trajectory for each DoF. All graphs report the dispersion of the data with a violin plot, with the median of each condition marked in white for both prostheses users involved. The table in (**E**) reports some of the main results of the online experiments and the participant survey scores. The questions preference score only considers questions where participants showed preference for one controller over the other for a one-point (or more) difference in Likert scale.

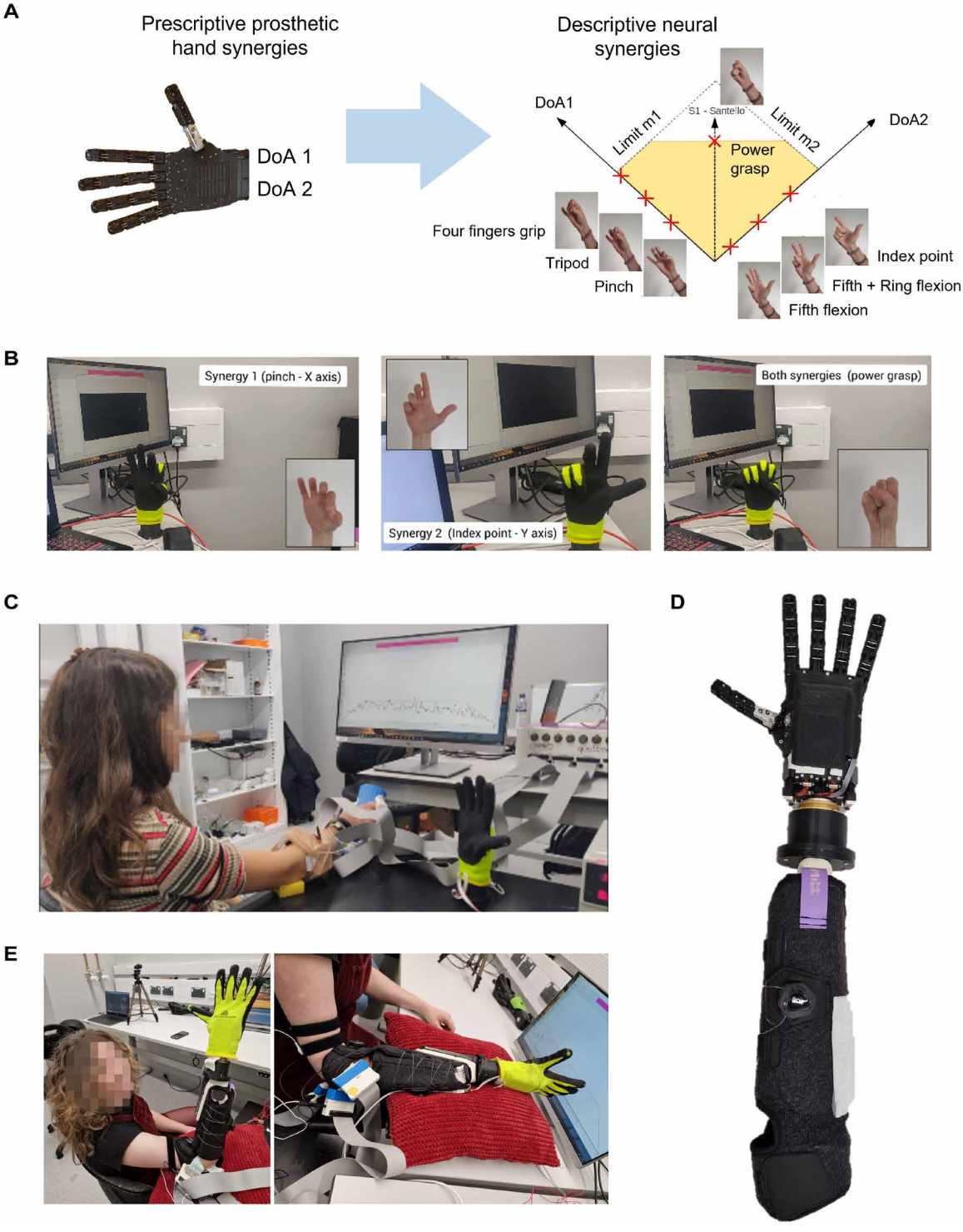

Fig. 8. Offline and online experimental protocol. (**A**) The seven hand postures, p_i, and their implementation in the prosthetic workspace. In this approach, we designed the full solution starting with prescriptive hand synergies (imposed by the available motions in the robot) to the descriptive neural synergies observed for p_i. (**B**) The online experiments during which a participant was asked to perform a virtual center-out target reaching task. (**C**) The recording framework for HD-sEMG data and the target trajectory to execute during the isometric muscle recordings. (**D**) Integration of the soft multisynergistic hand and a soft socket. (**E**) The full system integration showing the combination of HD-sEMG sensors on a soft socket, the soft multisynergistic hand, and the real-time neural synergistic control.

integrated system with PUs exploring finger movement coordination and voluntary in-hand manipulation with a bottle. During these demonstrations, PU1 reported the following "In particular, I see the potential of changing grasp without interruptions, but with a fluid movement. It was the first time I experienced such naturalness in going from 'point' to 'pinch' smoothly."

DISCUSSION

The selection of appropriate prescriptive synergies, which are those prescribed and fixed by the existing control system, is a difficult task during the design of robotic devices. The observed behavior in humans does not necessarily reveal the required control used by the nervous system, i.e., the prescriptive neural synergies (*14*). This was explored in this work introducing an approach to prosthetic design and bionic interfacing that combines postural and neural synergies. We hypothesized that the identification of more specific and controllable grasping coordination patterns, from MN synergies, could represent a robust and natural bionic interfacing method.

The Pisa/IIT SoftHand (*9*) was designed through the concept of postural synergies. It implemented only the first human hand synergy observed in grasping and hence explored a 1D space of hand postures (*13*). The earlier developed prosthetic version, the SoftHand Pro, realized a vast range of grasps and improved adaptability because of physical compliance and synergistic actuation through a tendon-driven differential mechanism. Despite its effectiveness in many practical conditions involving prehension, which were tested in clinical environments (*23*), this artificial hand presented limitations in dexterity when compared with a natural hand. Recent advances in prosthetics, e.g., the Hannes hand, have been characterized by similar attributes, such as high underactuation architectures (*24*). Nonetheless, the Hannes hand does not present characteristics of self-adapting mechanisms. In contrast, alternative hand prototypes may encompass elements of soft robotics technologies, yet they fall short in integrating postural synergies into their actuation architecture (*25, 26*). In addition, none of these hands explored more than one synergistic behavior. Consequently, our work merged synergies at both the hardware and software levels, which is a feature absent in other systems.

The multisynergistic hand development aims to generate additional motions and in-hand manipulation capabilities. The framework, initially developed for industrial robotic hands (*27*), underwent a preliminary study (*28*) to assess the feasibility of using a pair of EMG sensors and distinct signal maps for its control. The authors in (*29*) preliminarily explored the potential for proportional and simultaneous control through an off-the-shelf low-cost multichannel system with eight sEMG sensors (MYO Arm Band). Then, a human study was conducted to investigate the advantages of using a multisynergistic hand, leveraging an adapted pattern recognition classifier (*12*). We redesigned the system into the SoftHand Pro-2 for prosthetic applications. SoftHand Pro-2 resembles the human hand in shape, size, and functionality.

This study does not advance conventional myocontrol algorithms, which would typically warrant a comparative analysis. The pattern classification involves sequentially switching between DOFs (or grasps), which is fundamentally different from the continuous and proportional control of multiple DOFs with various synergies. We are pursuing the latter approach, because we believe that it is the crucial step toward achieving in-hand manipulation. Classic regression methods, on the other hand, would require labeling based on the kinematics, which is not required by the proposed synergistic approach. Therefore, it was deemed suitable to compare neural synergistic control with its closest version in the literature, muscle synergistic control, rather than with other alternatives. Although pattern recognition or standard regression techniques might satisfactorily govern two DoAs of a prosthetic device (*30*), the innovation presented herein lies in the use of a synergistic control methodology. The vision of associating this mechatronic design to specific neural structures is different from any other current approach to prosthesis design. Moreover, with respect to other maps, the modular structures extracted by MNs are stable when decoded from different MUs. This has been demonstrated in a previous study, where the use of muscle synergies allowed for robust control over different sessions (*31*). A generic map between MU spike trains and hand activation commands would need to be retrained for each use, whereas the identification of the latent small dimensionality in MU control can be done from any MU because the latent low-dimensional modules are invariant across the subset of units used for their determination (*32*).

The offline analysis indicated that MN synergies presented high dimensionality and specific information on the different grasping tasks involved, which included individual finger movements for the control of in-hand manipulation of the prosthesis. A greater number of synergies is not necessarily a preferred condition in synergy analysis. However, a higher dimensionality and greater degree of orthogonality is desirable for the design of controllers. The results in greater dimensionality and less redundancy of MN synergies with respect to muscle synergies are likely because of the very poor spatial selectivity of the interference EMG, which cannot be used to accurately identify neural control signals. The specificity observed in MN synergies during the offline analysis (see Fig. 4C) emphasizes the importance of selecting an appropriate number of MN synergies to maximize the available information to control the artificial limb in real time. The results from the online analysis, both in participants without physical impairment and PUs, suggested a larger controllable space for MN synergies and a more natural control. Our results indicate smooth transitions between MN synergies, which may be associated with better-coordinated multidigit actions. Furthermore, we conducted preliminary demonstrations with three PUs involving actions such as grasping and lifting and very simple manipulation of in-hand objects (Fig. 8, D and E). Although these tests were limited to simple tasks, as showcased in movies S1 and S2 for two of the three users, they provide preliminary evidence of some level of manipulation not possible with other systems.

The synergy extraction process involved seven specific voluntary movements predominantly characterized by coordinated and selective coactivation of flexor and extensor muscles for digit control. These chosen movements are a relatively constrained spectrum of actions achievable by the prosthesis. This was a deliberate choice, driven by the objective of assessing the preexisting MN synergies that directly correlate with the movements replicable by the robotic system. The primary focus of this work was to establish a direct map between the available robotic movements and the identified synergies rather than conducting a broad exploration of neural synergies across more complex human hand movements. The chosen map considers the specific requirements from both the robotic design and the decoded neural signals, adhering to the concepts of low-dimensional control by the CNS (*33, 34*) and the low-dimensional postural hand synergies (*13*) regulating the general shape of the hand. Our approach provides simple control of a soft underactuated hand with a large space of hand postures, contrary to classical approaches.

Considering the distinct limb pathologies of the PUs, we assume substantial differences in the accessibility of various muscles within the recorded residual limb. However, our methodology was designed to maximize the representation of extrinsic hand muscles in

the recorded data, aiming to identify the optimal number of synergies for both muscles and MNs regardless of their specific spatial locations. The effectiveness of this approach was demonstrated by the consistent performance and positive feedback reported by the PUs. Accordingly, this strategy guarantees adaptability in terms of muscle coverage, making it well suited for accommodating users with diverse muscle attributes and various surgical interventions.

The proposed codesign approach was tested on three PUs, two of whom are individuals with congenital limb malformation. Because these individuals never developed the required neural resources for controlling the missing limb, they may not have been able to provide the neural commands required for the proposed approach (*35*). However, both our offline and online experiments with the individuals with congenital limb malformation demonstrated outcomes consistent with those observed in participants without physical impairment and in the PU with transradial amputation. These observations indicate the potential of MN synergies as an alternative bionic interfacing, including in cases of congenital limb malformation.

Overall, our results validate the potential of the use of neural synergies to control postural synergies embedded in a prosthetic hand. This vision is an alternative bionic interfacing approach that could permit more advanced and natural in-hand manipulation skills. Although we included testing with two PUs and demonstrated the fully integrated framework with all three PUs, further investigations are needed to fully prove the usability of neural synergistic information and its application beyond laboratory settings. Moreover, future studies should aim at understanding the human capacity to flexibly control MN synergies by the CNS (*36*).

In conclusion, we demonstrated a method for natural bionic design and interfacing that controls the postural synergies of a prosthetic hand through neural synergies of spinal MNs. We demonstrated that synergistic codesign of robotic hands and neural information extraction algorithms can provide the users a natural modular control that spans infinite postures across a 2D space while reducing the complexity in the physical robotic device and in the control algorithms. This approach may lead to the design and control of bionic limbs that allow a greater degree of dexterity than previously possible.

MATERIALS AND METHODS

Offline analysis

Nine participants without physical impairments (28.4 ± 3.3 years old, six males and three females) participated in the experiments. They signed an informed consent form in accordance with the Declaration of Helsinki and approved by the Imperial College London Research Ethics Committee (reference number 18IC4685). The different grip tasks included in the protocol were verbally explained to them. No motion recording or force sensors were used. The exerted force contraction level for each grip task was estimated from the amplitude of the EMG.

We defined seven grip types or hand postures, p_i, where i indicates the chronological order of the grips during the recordings. These are shown in Fig. 8A together with their implementation in the proposed prosthetic system theoretical workspace. These included the flexions of the fifth digit or little finger (p_1), the fifth and the ring fingers (p_2), or the fifth, ring, and middle fingers (p_3, index point); flexion of all digits to apply force and make contact with the palm of the hand (p_4, power grasp); or making a contact with the thumb in opposition with the index finger (p_5, pinch), the index and middle fingers (p_6, tripod), and index to ring fingers (p_7).

Participants sat with the elbow flexed 90° to rest the weight of the arm on a table. The wrist and hand area were free to move, and the participant's arm rested over a piece of foam. They exerted isometric forces during all p_i at full closure. We recorded HD-sEMG from the upper forearm muscles controlling the digits. Three 64-channel grids with electrodes arranged in an eight-by-eight configuration were placed over the extrinsic extensor and flexor muscles of the hand. The interelectrode distance (IED) was 10 mm. For participants with smaller forearm circumference, two 64-channel 10-mm IED and one 64-channel 8-mm IED HD-sEMG grids were used. The reference and ground electrodes were placed at the wrist.

Monopolar HD-sEMG was recorded (Quattrocento, OT Bioelettronica), amplified with a gain of 150, bandpass filtered between 10 and 500 Hz, sampled at 2048 Hz, and A/D converted to 16 bits. Then, a 20- to 500-Hz digital bandpass filter was applied. The maximum voluntary contraction (MVC) of each grip was measured through the estimated EMG amplitude. This was estimated from each EMG window (window length of 128 samples, i.e., 62.5 ms) by first computing the root-mean-squared value of each EMG channel and then selecting the median value. This signal was then lowpass filtered with a fourth-order Butterworth filter with a cutoff frequency of 2.5 Hz. The MVC was used as a reference to determine the submaximal target contraction level in the trial. After the MVCs, the participants followed a target on a screen with a positive ramp (1% MVC/s), followed by a 20-s isometric contraction at 15% of MVC and a final negative ramp (1% MVC/s). A custom biofeedback application [presented in (*20*)] developed in MATLAB (MathWorks) was used to record the EMG signals, display the target force on a monitor in front of the participants, and provide them with visual feedback of the average muscle contraction exerted during each trial. A total of 63 recordings were included in the analysis.

After the EMG acquisition, recorded raw EMG signals were digitally band pass filtered (20 and 500 Hz, fourth-order Butterworth), concatenated (192 channels by 350 s) across all grip types, and decomposed to extract the spiking activity of individual MUs. Concatenation of EMG signals across all grip types was done to ensure consistent detection and tracking of MUs. After EMG decomposition, we applied NMF to the smoothed MU discharges to compute the MN synergies and observe the neural synergistic information. Then, we proposed a mathematical relation between the p_i, which was feasible to replicate with the hardware, and the extracted MN synergies. Hence, we defined the motor inputs or control commands for the prosthesis that achieved an appropriate mapping of the participant intentions into robotic postures. Figure 3A shows some examples of HD-sEMG recordings and the corresponding p_i. Figure 3B presents some examples of extracted spiking activity of individual MUs. We compared MN synergies to a standard control alternative, muscle synergies (termed MS in figures). For extracting muscle synergies, we applied NMF to different configurations of EMG signals, such as all monopolar or different combinations of bipolar channels. Before NMF factorization, we rectified the EMG signals and smoothed them with the same filter applied to the MNs smoothed discharge rates (SDRs). Figure 3 (C and D) shows the smoothed signals that were factorized using NMF to extract muscle and MN synergies, respectively.

EMG signal decomposition

This approach was based on HD-sEMG recordings using tens to hundreds of electrodes inserted in the muscle or mounted on the skin (*37*). Because of the spatial sampling over multiple locations,

HD-sEMG permits the identification of multiple MU activations simultaneously (*38*). It is possible to identify and decode the behavior of relatively large samples of one or more pools of active MNs during natural tasks [e.g., (*39*)]. This technique was based on a convolutive blind-source separation approach (*37*), which separates signal mixtures into the constituent components, identified as MUs.

In this experiment, we used a computationally efficient real-time interface [first introduced in (*19*)] based on the decoding of the activity of spinal MNs from wearable HD-sEMG sensors. Barsakcioglu *et al.* (*20*) validated this interface by comparing its decoding results with those obtained with invasive EMG sensors and offline decoding, as reference. Their results on accuracy, intuitiveness, and stability of control demonstrated the possibility of establishing a direct non-invasive neural interface with the spinal cord without the need for extensive training. The output of the interface is a binary sequence representing each individual MU spike train, with 1 indicating the occurrence of a spike and 0 otherwise (see Fig. 3B). The binary sequence of spikes for each detected MU was smoothed by a fourth-order Butterworth lowpass filter with cutoff frequency of 2.5 Hz and then normalized to 1. As previously used [e.g., (*40*)], this frequency bandwidth corresponds to a 400-ms Hanning window. The SDRs provide an estimation of the instantaneous firing rate for each MU (*41*).

Synergy extraction by NMF

To test the hypothesis of a low-dimensional representation of MN activity, we factorized motor neuron SDRs and monopolar or bipolar EMG envelopes using NMF. This is one of the most common methods in the literature for extraction of muscle synergies and makes no explicit assumption about correlation (*6*). We use the term "MN synergies" to indicate the time-invariant weights extracted by factorization of motor neuron SDRs [as in (*7*)] and "muscle synergies" to indicate the weights identified with the same factorization method applied to corresponding group of EMG envelopes [find other examples in (*2, 42*)]. For selecting the bipolar EMG channels, we did not assume any of the muscles' belly positioned consistently in a particular area. We used the same subdivision among participants with the same number and type of grids. We assumed that the forearm of each participant was completely covered by EMG channels and the subdivisions of the grids represented bands of different width and number of EMG sensors. For extracting MN synergies, a muscle assignment procedure was not required, and it did not affect the NMF analysis, because MNs from all the muscles were factorized as a unique pool (i.e., without grouping).

Let $\mathbf{V} \in \mathbb{R}^{M \times L}$ be the original matrix containing either the SDRs of the MNs or the EMG envelopes. L is the duration of the signals in samples, and M is the number of SDRs or the EMG envelopes. The NMF represents $\mathbf{V}$ as follows (*43*)

$$\mathbf{V} \approx \mathrm{WH} \tag{1}$$

where $\mathbf{W} \in \mathbb{R}^{M \times S}$ is the matrix of the time-invariant synergy coefficients and $\mathbf{H} \in \mathbb{R}^{S \times L}$ is the matrix of the activation signals, with S being the number of extracted synergies. Whereas the time-invariant $\mathbf{W}$ represents, for each column, how an MN (or EMG sensor) contributes to each synergy, $\mathbf{H}$ contains the time-varying activation of each synergy during the production of isometric forces during the execution of the hand patterns (p_i).

NMF is an iterative process that minimizes the Euclidean distance between the original signals $\mathbf{V}$ and the reconstruction obtained by the multiplication of $\mathbf{W}$ and $\mathbf{H}$. In this study, the NMF iterations (100 were chosen) were repeated 10 times for each number of synergies, i.e., from one to nine synergies, with different seeds per repetition for the matrices $\mathbf{W}$ and $\mathbf{H}$. The reconstruction of the original dataset ($\mathbf{V}$) by $\mathbf{W}$ and $\mathbf{H}$ was quantified with the coefficient of determination (R^2), as done in (*44*). The greatest R^2 among the 10 repetitions with different seeds was retained for each number of synergies. An example of the resulting $\mathbf{W}$ and $\mathbf{H}$ matrices is visible in Fig. 3, both from MUs (Fig. 3C) and sEMG recordings (Fig. 3D). Figure 3 (G and H) shows examples of the muscle and MU activations reconstructed from the extracted synergies, as well as their original rectified EMG or SDR signals, respectively. No attempt was made to record conventional, muscle-specific EMG signals or to relate the extracted muscle EMG signals to anatomical muscles or functions. This approach was deemed suitable within the experimental framework, given the potential variability in sensor placement among participants and its dependence on the individual forearm dimensions. Thus, the decision was made to cover the extrinsic hand muscles to the greatest extent possible and to extract an optimal number of synergies for both muscles and MNs independently of their locations. This approach was also regarded as appropriate to enhance the adaptability of the methodology across patients with varying muscle attributes or diverse surgical interventions.

Analysis

Different types of synergies were compared in relation to their redundancy and information content. First, we determined the required synergy dimensionality for both MNs and muscles. The required number of synergies in each case was identified from the R^2 curve with a cutoff threshold of 0.8 or, alternatively, from the MSE curve with a threshold of 5×10^{-4} (*6, 45*). For muscle synergy extraction, we tried nine different sensor configurations (minimum of 12 bipolar to 192 monopolar). Forty-eight bipolar sEMG sensors were selected for the following analysis and the online control. We evaluated the orthogonality between the pairs of synergies from the same dataset as an indication of the specificity of the information carried by each synergy. For this purpose, we computed the pairwise dot product between synergies divided by the length of each of the vectors.

We evaluated the orthogonality for three sets of synergies for both muscles and MNs. The first was the set of synergies obtained by the analysis of the R^2 curve separately for muscles and MNs (set I). The second comprised the number of synergies identified by the R^2 curve for the MNs, and the same number was imposed for the muscle synergies (set II). The third comprised the number of synergies identified by the R^2 curve for the muscle activities, and the same number was imposed for the MN synergies (set III). Last, we also investigated the correlation coefficient among time-varying activation synergies from different sets to compute the degree of similarity in best-matching synergy pairs.

Online validation

Eleven participants without physical impairment (27.3 ± 2.9 years old, four males and seven females) and two PUs participated in the experiments. They signed an informed consent form in accordance with the Declaration of Helsinki and approved by the Imperial College London Research Ethics Committee (reference number 18IC4685). Three of the participants without physical impairment had also participated in the previous offline experiment. The experiment was a within-participant study. Hence, participants individually tested our algorithms in a designed experiment for approximately 90 min.

Figure 8 (B and C) shows the online experiment setup. HD-sEMG sensors were placed covering the muscles of the upper forearm given that this is a common targeted area for transradial amputees. A conductive paste was used to improve the electrode-skin contact. Before sensor placement, the skin above the target muscle was shaved and cleaned of dead skin, dirt, and dust particles with an abrasive paste and alcohol. The HD-sEMG signals were monopolar recorded, amplified, filtered (10 to 500 Hz), sampled at 2048 Hz, and A/D converted to 16 bits. A further digital bandpass filter (20 to 500 Hz) was also applied. The data were acquired in the form of 128 samples/channel packets (i.e., a 62.5-ms length for each packet).

The setup featured a finger handle with the arm resting on the table to ensure fixed hand position and to facilitate isometric force contractions, a custom-designed graphical user interface for providing feedback to the user and the experimenter, a desktop-mounted SoftHand Pro-2, and a virtual environment for 2D center-out target reaching tasks. The virtual control space was mapped to the individual finger movements for evaluating control task performance and individual skills for in-hand manipulation. The finger handle allowed a closer resemblance to recording in PUs, where no limb movements are possible. Figure 8C shows an example of a participant without physical impairment. The movement of the cursor corresponded to a potential configuration of the prosthesis. The inclusion of the SoftHand Pro-2 as visual feedback during the familiarization phase and experiments aimed to evaluate the intuitiveness of the control mapping. Note that the prosthesis correctly executed the intended patterns, close to what a human hand would do; see Fig. 8B. Last, note that pinch and index point corresponded to opposite axes in the virtual prosthesis, given that they occur with the opposite rotation direction of the fingers. The power grasp, on the other hand, was represented by the diagonal of the 2D virtual space and the combination of both axes.

The experimental protocol started with measuring the MVC of the pinch grasp task. The EMG amplitude during the MVC of the pinch grasp task was used to normalize the EMG feedback. This allowed the extraction of synergies from each hand posture at similar contraction levels. This was to avoid large variations in the contraction levels for different postures (e.g., hand grasp versus little finger), which might result in neglecting the synergistic contribution of the lower muscle activations in certain static hand postures. After the MVC measurement, participants were presented with a series of seven trapezoidal traces for different static hand postures as described in the offline analysis. Each trapezoidal trace consisted of a 5-s ramp trajectory, followed by a constant 30% MVC trajectory sustained over 15 s and a descending ramp again of 5 s. The visual feedback on the contraction level was provided by plotting the median of the envelopes from all recorded EMG channels. The HD-sEMG signals recorded during the seven trapezoidal traces were used as the training data for computing the online decomposition parameters.

After the training of online decomposition, the control algorithm was trained. The training started with asking participants to follow, with the provided visual feedback, a target trajectory for the seven actions described above. Each target trajectory consisted of a 5-s ramp trajectory followed by a constant 30% MVC trajectory sustained over 5 s and a descending ramp of 5 s. The recorded HD-sEMG signals were then used to extract the corresponding neural and muscle synergies through NMF factorization. The extracted synergies were mapped onto two directions in the first quadrant of a 2D space, which corresponded to the two DoAs of the SoftHand Pro-2. This map, shown in Fig. 5, involved the estimation of a linear regression model that mapped the global activation of the motors onto the presented 2D space.

Before the start of the online control task, participants were asked to explore different strategies to command a cursor in the 2D space by activating different synergies (familiarization phase), as well as exploring the prosthesis workspace simultaneously and proportionally. The online control task was a center-out target reaching task, during which the participants were asked to move the cursor into the target position and hold it there for at least 640 samples (312.5 ms, five buffers). The targets were fixed positions within the first quadrant of the 2D space and were presented to the participants in randomly selected order. A total of 20 targets were presented, and participants had 20 s to perform the desired target hit for each target. The targets were chosen to include positions spanning the complete workspace, encompassing specific in-hand manipulation poses. Between each target, the participants were asked to relax their muscles, which brought the cursor to the origin. This was repeated for both control methods (neural and muscle synergies) in a randomized order among participants. After the 2D control task, participants were asked to respond to a customized survey regarding the usability of the control methods.

Analysis metrics

Different metrics were selected to evaluate the performance of participants for the two control conditions tested during the online 2D virtual control experiments. For all targets, we computed the normalized distance, d, between the cursor and the target positions as

$$d = \frac{\sqrt{\left(\left(\frac{x_{\text{target}} - x_{\text{cmd}}}{x_{\max}}\right) * 100\right)^2 + \left(\left(\frac{y_{\text{target}} - y_{\text{cmd}}}{y_{\max}}\right) * 100\right)^2}}{2} \quad (2)$$

where x_{target} and y_{target} are the target positions, and x_{cmd} and y_{cmd} are the cursor positions. $x_{\max}$ and $y_{\max}$ indicate the range for each axis. We report both the median and the minimal distance. We also computed the execution time for reachable and for successful target hits. In the case of successful target hits, the execution time was computed from the starting time to the first instant in which the target was hit and the position was held for 312.5 ms. Last, we also evaluated the variability of the commanded cursor trajectory through the SD of the error and the first derivate of the error for each axis.

Prosthesis user protocol

Offline and online experiments were also conducted with PUs. PU1 and PU3 are individuals with congenital limb malformation, and PU2 is a transradial amputee. For the offline analysis (only with PU1), three recording conditions were chosen to analyze MN and muscle synergies. HD-sEMG signals were recorded from the intact limb while PU1 was actively executing the various grasping patterns (similar to the offline protocol with participants without physical impairment), from the intact limb while PU1 was grasping a custom-designed handle to enforce isometric contractions (similar to the online experiment with participants without physical impairment), and from the residual limb while PU1 imagined executing hand movements with the missing hand. For the latter recording condition, PU1 was also asked to simultaneously execute the same action

with the intact hand. Between each offline session, 60 min of break was introduced to minimize muscle fatigue. During a second day of experiments with PU1, the online experiment protocol was executed. The experiment protocol was similar to the one with participants without physical impairment; however, PU1 was allowed a maximum of 40 s to hit the targets instead of 20 s. The HD-sEMG signals were recorded only from the residual limb. The online experiment was also repeated with PU2. Last, we validated our approach with all three PUs by fully integrating the control algorithm, the developed prosthesis, and a soft socket lined with HD-sEMG sensors. The latter step permitted the exploration of the new features and real-time in-hand manipulation of objects and demonstrated the proposed technology.

Statistics

The collected data were analyzed using MATLAB R2023b (MathWorks Inc.). The results are presented as mean ± SD unless otherwise specified. To evaluate the control performance and survey scores for both offline and online analyses, two-sample t tests were used to compare the main experimental conditions: muscle synergies and MN synergies. The significance level was set at 0.05. Figure captions include the statistical tests performed for each analysis, along with their significance values. For the real-time controller evaluations, violin plots were used to display data dispersion.

Supplementary Materials

The PDF file includes:
Table S1
Fig. S1

Other Supplementary Material for this manuscript includes the following:
Movies S1 and S2
MDAR Reproducibility Checklist

REFERENCES AND NOTES

1. A. D'Avella, M. Giese, Y. P. Ivanenko, T. Schack, T. Flash, Editorial: Modularity in motor control: From muscle synergies to cognitive action representation. *Front. Comput. Neurosci.* **9**, 10.3389/fncom.2015.00126 (2015).
2. E. Bizzi, V. C. K. Cheung, A. d'Avella, P. Saltiel, M. Tresch, Combining modules for movement. *Brain Res. Rev.* **57**, 125–133 (2008).
3. A. D'Avella, A. Portone, L. Fernandez, F. Lacquaniti, Control of fast-reaching movements by muscle synergy combinations. *J. Neurosci.* **26**, 7791–7810 (2006).
4. E. J. Weiss, M. Flanders, Muscular and postural synergies of the human hand. *J. Neurophysiol.* **92**, 523–535 (2004).
5. A. B. Ajiboye, R. F. Weir, Muscle synergies as a predictive framework for the EMG patterns of new hand postures. *J. Neural Eng.* **6**, 036004 (2009).
6. M. C. Tresch, V. C. K. Cheung, A. Avella, C. Matthew, V. C. K. Cheung, A. Avella, Matrix factorization algorithms for the identification of muscle synergies: Evaluation on simulated and experimental data sets. *J. Neurophysiol.* **95**, 2199–2212 (2006).
7. S. Tanzarella, S. Muceli, M. Santello, D. Farina, Synergistic organization of neural inputs from spinal motor neurons to extrinsic and intrinsic hand muscles. *J. Neurosci.* **41**, 6878–6891 (2021).
8. M. Santello, G. Baud-Bovy, H. Jörntell, Neural bases of hand synergies. *Front. Comput. Neurosci.* **7**, 23 (2013).
9. M. G. Catalano, G. Grioli, E. Farnioli, A. Serio, C. Piazza, A. Bicchi, Adaptive synergies for the design and control of the Pisa/IIT SoftHand. *Int. J. Robot. Res.* **33**, 768–782 (2014).
10. E. Bizzi, V. C. K. Cheung, The neural origin of muscle synergies. *Front. Comput. Neurosci.* **7**, 51 (2013).
11. S. Madarshahian, J. Letizi, M. L. Latash, Synergic control of a single muscle: The example of flexor digitorum superficialis. *J. Physiol.* **599**, 1261–1279 (2021).
12. C. Piazza, A. M. Simon, K. L. Turner, L. A. Miller, M. G. Catalano, A. Bicchi, L. J. Hargrove, Exploring augmented grasping capabilities in a multi-synergistic soft bionic hand. *J. Neuroeng. Rehabil.* **17**, 116 (2020).
13. M. Santello, M. Flanders, J. F. Soechting, Postural hand synergies for tool use. *J. Neurosci.* **18**, 10105–10115 (1998).
14. O. Brock, F. Valero-Cuevas, Transferring synergies from neuroscience to robotics. *Phys. Life Rev.* **17**, 27–32 (2016).
15. A. Bicchi, M. Gabiccini, M. Santello, Modelling natural and artificial hands with synergies. *Philos. Trans. R. Soc. B Biol. Sci.* **366**, 3153–3161 (2011).
16. F. Hara, R. Pfeifer, *Morpho-Functional Machines: The New Species* (Springer Science and Business Media, 2003).
17. M. L. Latash, S. Gorniak, V. M. Zatsiorsky, Hierarchies of synergies in human movements. *Kinesiology* **40**, 29–38 (2008).
18. V. C. K. Cheung, A. D'Avella, M. C. Tresch, E. Bizzi, Central and sensory contributions to the activation and organization of muscle synergies during natural motor behaviors. *J. Neurosci.* **25**, 6419–6434 (2005).
19. D. Y. Barsakcioglu, D. Farina, A real-time surface EMG decomposition system for non-invasive human-machine interfaces, in *2018 IEEE Biomedical Circuits and Systems Conference, BioCAS 2018 - Proceedings* (IEEE, 2018), pp. 10–13.
20. D. Y. Barsakcioglu, M. Bracklein, A. Holobar, D. Farina, Control of spinal motoneurons by feedback from a non-invasive real-time interface. *IEEE Trans. Biomed. Eng.* **68**, 926–935 (2021).
21. C. Lin, B. Wang, N. Jiang, D. Farina, Robust extraction of basis functions for simultaneous and proportional myoelectric control via sparse non-negative matrix factorization. *J. Neural Eng.* **15**, 026017 (2018).
22. N. Jiang, I. Vujaklija, H. Rehbaum, B. Graimann, D. Farina, Is accurate mapping of EMG signals on kinematics needed for precise online myoelectric control? *IEEE Trans. Neural Syst. Rehabil. Eng.* **22**, 549–558 (2014).
23. P. Capsi-Morales, C. Piazza, M. G. Catalano, G. Grioli, L. Schiavon, E. Fiaschi, A. Bicchi, Comparison between rigid and soft poly-articulated prosthetic hands in non-expert myo-electric users shows advantages of soft robotics. *Sci. Rep.* **11**, 23952 (2021).
24. M. Laffranchi, N. Boccardo, S. Traverso, L. Lombardi, M. Canepa, A. Lince, M. Semprini, J. A. Saglia, A. Naceri, R. Sacchetti, E. Gruppioni, L. De Michieli, The Hannes hand prosthesis replicates the key biological properties of the human hand. *Sci. Robot.* **5**, eabb0467 (2020).
25. A. Mohammadi, J. Lavranos, H. Zhou, R. Mutlu, G. Alici, Y. Tan, P. Choong, D. Oetomo, A practical 3D-printed soft robotic prosthetic hand with multi-articulating capabilities. *PLOS ONE* **15**, e0232766 (2020).
26. G. Gu, N. Zhang, H. Xu, S. Lin, Y. Yu, G. Chai, L. Ge, H. Yang, Q. Shao, X. Sheng, X. Zhu, X. Zhao, A soft neuroprosthetic hand providing simultaneous myoelectric control and tactile feedback. *Nat. Biomed. Eng.* **7**, 589–598 (2023).
27. C. Della Santina, C. Piazza, G. Grioli, M. G. Catalano, A. Bicchi, Toward dexterous manipulation with augmented adaptive synergies: The Pisa/IIT SoftHand 2. *IEEE Trans. Robot.* **34**, 1141–1156 (2018).
28. M. Maimeri, C. Della Santina, C. Piazza, M. Rossi, M. G. Catalano, G. Grioli, Design and assessment of control maps for multi-channel sEMG-driven prostheses and supernumerary limbs. *Front. Neurorobot.* **13**, 10.3389/fnbot.2019.00026 (2019).
29. M. Rossi, C. Della Santina, C. Piazza, G. Grioli, M. Catalano, A. Bicchi, "Preliminary Results toward a Naturally Controlled Multi-Synergistic Prosthetic Hand" in *2017 International Conference on Rehabilitation Robotics (ICORR)* (IEEE, 2017), pp. 1356–1363.
30. M. Nowak, I. Vujaklija, A. Sturma, C. Castellini, D. Farina, Simultaneous and proportional real-time myocontrol of up to three degrees of freedom of the wrist and hand. *IEEE Trans. Biomed. Eng.* **70**, 459–469 (2023).
31. J. M. Hahne, M. A. Schweisfurth, M. Koppe, D. Farina, Simultaneous control of multiple functions of bionic hand prostheses: Performance and robustness in end users. *Sci. Robot.* **3**, eaat3630 (2018).
32. F. Hug, S. Avrillon, J. Ibáñez, D. Farina, J. Physiol, Common synaptic input, synergies and size principle: Control of spinal motor neurons for movement generation. *J. Physiol.* **601**, 11–20 (2023).
33. J. J. Kutch, F. J. Valero-Cuevas, Challenges and new approaches to proving the existence of muscle synergies of neural origin. *PLoS Comput. Biol.* **8**, 10.1371/journal.pcbi.1002434 (2012).
34. V. C. K. Cheung, K. Seki, Approaches to revealing the neural basis of muscle synergies: A review and a critique. *J. Neurophysiol.* **125**, 1580–1597 (2021).
35. T. R. Makin, F. de Vignemont, S. Micera, Soft embodiment for engineering artificial limbs. *Trends Cogn. Sci.* **24**, 965–968 (2020).
36. M. L. Latash, V. Krishnamoorthy, J. P. Scholz, V. M. Zatsiorsky, Postural synergies and their development. *Neural Plast.* **12**, 119–130 (2005).
37. A. Holobar, D. Farina, M. Gazzoni, R. Merletti, D. Zazula, Estimating motor unit discharge patterns from high-density surface electromyogram. *Clin. Neurophysiol.* **120**, 551–562 (2009).
38. F. Negro, S. Muceli, A. M. Castronovo, A. Holobar, D. Farina, Multi-channel intramuscular and surface EMG decomposition by convolutive blind source separation. *J. Neural Eng.* **13**, 026027 (2016).
39. D. Farina, I. Vujaklija, M. Sartori, T. Kapelner, F. Negro, N. Jiang, K. Bergmeister, A. Andalib, J. Principe, O. C. Aszmann, Man/machine interface based on the discharge timings of spinal motor neurons after targeted muscle reinnervation. *Nat. Biomed. Eng.* **1**, 0025 (2017).

40. F. Negro, A. Holobar, D. Farina, Fluctuations in isometric muscle force can be described by one linear projection of low-frequency components of motor unit discharge rates. *J. Physiol.* **587**, 5925–5938 (2009).
41. C. J. De Luca, R. S. Lefever, M. P. Mccue, A. P. Xenakis, Control scheme governing concurrently active human motor units during voluntary contractions. *J. Physiol.* **329**, 129–142 (1982).
42. V. C. K. Cheung, L. Piron, M. Agostini, S. Silvoni, A. Turolla, E. Bizzi, Stability of muscle synergies for voluntary actions after cortical stroke in humans. *Proc. Natl. Acad. Sci. U.S.A.* **106**, 19563–19568 (2009).
43. C. Févotte, J. Idier, Algorithms for nonnegative matrix factorization with the β-divergence. *Neural Comput.* **23**, 2421–2456 (2011).
44. S. Muceli, A. T. Boye, A. D'Avella, D. Farina, Identifying representative synergy matrices for describing muscular activation patterns during multidirectional reaching in the horizontal plane. *J. Neurophysiol.* **103**, 1532–1542 (2010).
45. A. D'avella, A. Portone, F. Lacquaniti, Superposition and modulation of muscle synergies for reaching in response to a change in target location. *J. Neurophysiol.* **106**, 2796–2812 (2011).

Acknowledgments: This work used expertise and prototyping equipment at the Imperial College Advanced Hackspace. We thank S. Tanzarella for fruitful discussions at the early stages of the project and M. Hasbani, J. Kashiwakura, and B. Baumgartner for the help in preparations for testing the integrated system. We also thank M. Poggiani and V. Tincani for the technical support on the development of the prosthetic hand device. **Funding:** This research has received funding from the European Union's Horizon 2020 ERC program under grant agreement no. 810346 (Natural Bionics). The content of this publication is the sole responsibility of the authors. The European Commission or its services cannot be held responsible for any use that may be made of the information it contains. This work has also been supported in part by the Italian Ministry of Research, under the complementary actions to the NRRP "Fit4MedRob - Fit for Medical Robotics" under grant PNC0000007. **Author contributions:** Conceptualization: P.C.-M., D.Y.B., M.G.C., G.G., A.B., and D.F. Methodology: P.C.-M., D.Y.B., and D.F. Formal analysis: P.C.-M. and D.Y.B. Investigation: P.C.-M., D.Y.B., A.B., and D.F. Resources: P.C.-M., D.Y.B., A.B., and D.F. Data curation: P.C.-M. and D.Y.B. Writing–original draft: P.C.-M. and D.Y.B. Writing–review and editing: P.C.-M., D.Y.B., M.G.C., G.G., A.B., and D.F. Visualization: P.C.-M. and D.Y.B. Supervision: A.B. and D.F. Project administration: M.G.C. and G.G. Funding acquisition: A.B. and D.F. **Competing interests:** P.C.-M., D.Y.B., and D.F. declare no competing interests. M.G.C., G.G., and A.B. are among the co-founders and shareholders of qbrobotics srl, a company producing robotic hands and components of the SoftHand Pro-2 used in the experiments reported in this paper. At the time of the publication of this manuscript, qbrobotics has a license agreement for the distribution of the SoftHand2. The SoftHand2 Pro is the prosthetic version of the robotic hand SoftHand2, which is patented under number EP3457995B1 by the European Patent Office. **Data and materials availability:** The main data supporting the results in this study are available within the paper or the Supplementary Materials. The data for this study have been deposited in the database https://doi.org/10.5281/zenodo.14275997.

Submitted 11 March 2024
Accepted 11 December 2024
Published 15 January 2025
10.1126/scirobotics.ado9509

Science Robotics

Merging motoneuron and postural synergies in prosthetic hand design for natural bionic interfacing

Patricia Capsi-Morales, Deren Y. Barsakcioglu, Manuel G. Catalano, Giorgio Grioli, Antonio Bicchi, and Dario Farina

Sci. Robot. **10** (98), eado9509. DOI: 10.1126/scirobotics.ado9509

Science Robotics (ISSN 2470-9476) is published by the American Association for the Advancement of Science. 1200 New York Avenue NW, Washington, DC 20005. The title *Science Robotics* is a registered trademark of AAAS.